ACS Catalysis

Research Article

pubs.acs.org/acscatalysis

Metadynamics-Biased ab Initio Molecular Dynamics Study of Heterogeneous CO_2 Reduction via Surface Frustrated Lewis Pairs

Mireille Ghoussoub,[†] Shwetank Yadav,[†] Kulbir Kaur Ghuman,[†] Geoffrey A. Ozin,[‡] and Chandra Veer Singh*[,†,§]

[†]Department of Materials Science and Engineering, University of Toronto, 184 College Street, Toronto, Ontario M5S 3E4, Canada

[‡]Department of Chemistry, University of Toronto, 80 St. George Street, Toronto, Ontario M5S 3H6, Canada

[§]Department of Mechanical and Industrial Engineering, University of Toronto, 5 King's College Road, Toronto, Ontario, M5S 3G8 Canada

Supporting Information

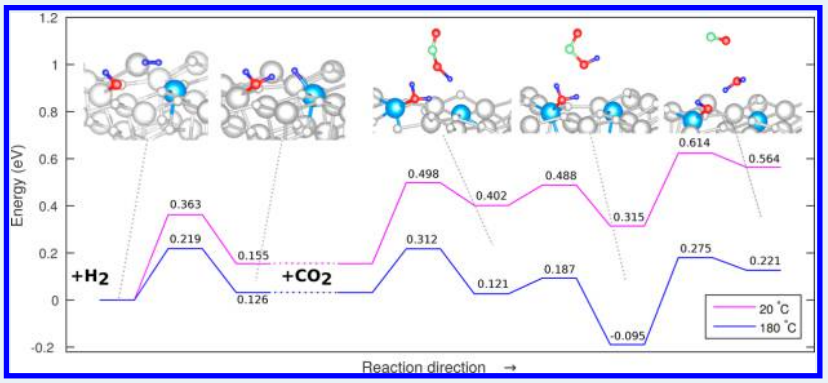

ABSTRACT: The recent discovery of frustrated Lewis pairs (FLPs) capable of heterolytically splitting hydrogen gas at the surface of hydroxylated indium oxide ($In_2O_{3-x}(OH)_y$) nanoparticles has led to interesting implications for heterogeneous catalytic reduction of CO_2. Although the role of surface FLPs in the reverse water-gas shift (RWGS) reaction ($CO_2 + H_2 \rightarrow CO + H_2O$) has been experimentally and theoretically demonstrated, the interplay between surface FLPs and temperature and their consequences for the reaction mechanism have yet to be understood. Here we use well-tempered metadynamics-biased ab initio molecular dynamics to obtain the free energy landscape of the multistep RWGS reaction at finite temperatures. The reaction is simulated at 20 and 180 °C, and the minimum energy reaction pathways and energy barriers corresponding to H_2 dissociation and CO_2 reduction are obtained. The reduction of CO_2 at the surface FLP catalytically active site, where H_2 is heterolytically dissociated and bound, is found to be the rate-limiting step and is mostly unaffected by increased temperature conditions; however, at 180 °C the energetic barriers associated with the splitting of H_2 and the subsequent adsorption of CO_2 are reduced by 0.15 and 0.19 eV, respectively. It is suggested that increased thermal conditions may enhance reactivity by enabling the surface FLP to become further spatially separated. Product H_2O is found to favor dissociative adsorption over direct desorption from the surface of $In_2O_{3-x}(OH)_y$ and may therefore impede sustained catalytic activity by blocking surface sites.

KEYWORDS: *CO_2 reduction, surface frustrated Lewis pairs, metadynamics, ab intio molecular dynamics, hydrogen dissociation, reverse water-gas shift reaction*

1. INTRODUCTION

In light of climate change and growing global energy demands, the conversion of greenhouse gas CO_2 into carbon-based fuels and chemical feedstocks may be the key to building a carbon-neutral sustainable economy.[1−3] The production of fuels, such as CH_4 and CH_3OH, requires splitting of gaseous CO_2, which has led to a widespread investigation by the scientific community to find a cheap and abundant catalyst material capable of efficient C−O bond cleavage.[4,5] The concept of frustrated Lewis pairs (FLPs), in which a sterically hindered Lewis acid−base pair forms a reactive site conducive to the activation of small molecules, offers an effective solution for CO_2 activation.[6,7] Unlike classical Lewis acids and bases that react to form Lewis adducts, the electronically unquenched nature of FLPs accords them a chemistry typically characteristic of transition metals, enabling them to heterolytically split H_2 and subsequently react with a variety of species, such as alkenes, aldehydes, and even carbon dioxide.[8,9] To date, FLP complexes have been demonstrated to reversibly bind CO_2,[10,11] as well as to stoichiometrically reduce CO_2 to CH_3OH,[12−15] CH_4,[16] and

Received: June 1, 2016
Revised: September 6, 2016
Published: September 13, 2016

DOI: 10.1021/acscatal.6b01545
ACS Catal. 2016, 6, 7109−7117

CO.[17] Their unique reactivity continues to find applications in new areas, such as transition-metal chemistry, bioinorganic chemistry, and materials science.[6,9] While the notion of FLPs has remained synonymic to molecular FLPs, the existence of FLP sites on the surface of a nanocrystalline hydroxylated indium oxide ($In_2O_{3-x}(OH)_y$) catalyst surface has recently been brought to light.[18−20] Semiconductor nanoparticles are well-suited to serve as photo- and thermocatalytic materials, given their favorable electronic properties. In this study, we seek a catalytic material with the ability to drive CO_2 chemistry; therefore, the appropriate candidate should exhibit surface sites capable of selectively reducing carbon dioxide, be sufficiently stable in reaction environments, and contain low selectivity for product oxidation. Indium sesquioxide (In_2O_3), renowned for its electronic, optical, and surface properties,[21,22] has been used as a chemical sensor[23] and has also been investigated for methanol steam re-forming;[24] however, the introduction of oxygen vacancies and surface hydroxides has been shown to create a promising catalyst capable of converting CO_2 to CO via the reverse water-gas shift (RWGS) reaction, $CO_2 + H_2 \rightarrow CO + H_2O$, at a rate of 150 μmol g^{-1} h^{-1}.[19] In the RWGS reaction, the surface FLP heterolytically splits gaseous H_2 and the resulting proton and hydride moieties are bound to a surface hydroxide group and an indium atom, creating a site suitable for CO_2 capture and reduction. In this process CO_2 is converted to CO and H_2O, which desorb to leave behind surface FLP sites accessible for further reactions. The rate of conversion of CO_2 to CO has been found to be 4 times greater under visible light conditions, and theoretical studies of ground and excited states have confirmed surface FLP chemistry to be key in driving both the thermochemical and photochemical reactions.[19,20]

In visible light, catalytic activity has been reported to increase from 15.4 μmol g^{-1} h^{-1} at 150 °C to 153 μmol g^{-1} h^{-1} at 180 °C, beyond which point the catalyst is reportedly no longer stable due to sintering of the nanoparticles. In dark conditions, practicable CO production is achieved at 165 °C and increases to 35.7 μmol g^{-1} h^{-1} at 180 °C.[19] While a multistep mechanism for the RWGS reaction based on ground state density functional theory (DFT) has been proposed, it does not capture changes in reaction paths that may proceed at finite temperature and the corresponding influences on energy barriers owing to entropic effects. In this study, we use well-tempered metadynamics-biased ab initio molecular dynamics to explore the free energy surface of surface FLP induced H_2 splitting, CO_2 reduction, and H_2O desorption over $In_2O_{3-x}(OH)_y$ with the objective of identifying the minimum free energy pathways, the corresponding activation energies, and the rate-limiting step of the reaction at finite temperatures. In addition, we provide grounds for the enhanced activity of the thermochemical RWGS reaction observed experimentally at higher temperature, derived from the thermal effects on surface FLP chemistry.

2. COMPUTATIONAL METHODS

In order to investigate the reaction mechanism at finite temperature, we performed ab initio molecular dynamics (AIMD) on the Born−Oppenheimer surface. The computationally expensive nature of these simulations restricts them to explore the system's dynamics over short durations only, and therefore AIMD alone is unable to capture full reactions of interest. This limitation is evaded by employing metadynamics (MetaD), a recently developed approach that applies a periodic bias to the system to encourage efficient, self-avoiding exploration of the free energy landscape.[25,26] MetaD has proven to be a useful tool for overcoming the sampling limitations of traditional molecular dynamics on complex molecular processes.[27−30] In this method, a history-dependent potential is added intermittently throughout the simulation to encourage efficient sampling of the associated free energy surface. The latter is defined over a set of collective variables (CVs), carefully selected to provide a complete description of the slow degrees of freedom of the system. The Helmholtz free energy surface corresponds to simulations carried out in the canonical ensemble (N, V, T) and therefore accounts for entropic contributions to the displacement of ions. The history-dependent bias takes the form of Gaussian functions to allow the system to escape beyond high energy barriers, thus allowing for faster sampling of the reaction surface.

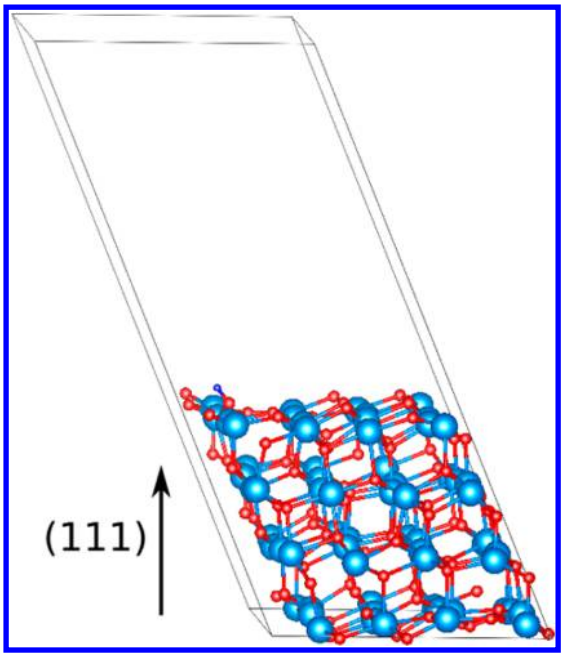

Figure 1. Side view of the $In_2O_{3-x}(OH)_y$ supercell. The light blue atoms denote indium, the red atoms denote oxygen, and the dark blue atoms denote hydrogen.

Throughout the study, AIMD simulations were performed with the Quantum Espresso software package[31] using the DFT plane-wave basis set approach. All calculations were spin-polarized and implemented using the Perdew−Burke−Ernzerhof (PBE) exchange correlation functional,[32] together with the Rappe−Rabe−Kaxiras−Joannopoulos (RRKJ) ultra-soft pseudopotentials.[33,34] Kinetic energy cutoffs were 50 and 400 Ry for the wave functions and charge density, respectively, and the criterion for self-consistent field convergence was set to 1×10^{-6} Ry. The choice of supercell is based on results from a previously conducted ground-state DFT study in which the locations of oxygen defects and hydroxyl groups in the $In_2O_3(111)$ supercell were rigorously tested at all possible sites to determine the most energetically favorable cell configuration. HR-STEM images of $In_2O_{3-x}(OH)_y$ nanocrystalline samples confirmed the presence of (111) planes.[19] On the basis of these results, the system modeled the nanofilm as a continuous four-layer slab with 160 atoms, roughly 11.5 Å in thickness, to capture the effect of nonedge nanocrystal regions (Figure 1).

DOI: 10.1021/acscatal.6b01545
ACS Catal. 2016, 6, 7109−7117

Brillouin zone integrations were performed over the γ point due to the large size of the supercell. After the complete structure at the ground-state configuration was converged initially, the bottom two layers were frozen in all AIMD calculations, while the top two layers and adsorbates were allowed to relax. Relaxation was performed using the conjugate gradient minimization algorithm until the magnitude of the residual Hellman−Feynman force on each atom was less than 1×10^{-3} Ry/bohr. The Anderson thermostat was used to maintain the temperature in all simulations. Each reaction step was investigated at 20 °C, in order to gain insight into its room-temperature feasibility and to serve as a reference temperature, and at 180 °C, which has been reported to be the temperature yielding highest activity.[19] It was previously reported that the catalyst nanoparticles do not maintain stability at temperatures above 200 °C due to sintering and loss of surface hydroxides reported above 250 °C, which limited the previous experimental investigations to 190 °C.[19] The highest reported rates were at ∼180 °C under dark conditions, and this therefore chosen as the reaction temperature for the study. Moreover, changes to the minimum reaction energy pathway, and their concomitant effects on transition-state structures, that result from increased thermal energy were captured by performing the simulations at different temperatures. A time step of 2.0 fs was taken for all AIMD simulations. This value was determined by performing multiple test simulations (see the Supporting Information) large enough to minimize computational cost of sampling the free energy surfaces yet sufficiently small to guarantee the accuracy of the Verlet algorithm. Well-tempered MetaD-biased simulations were carried out using the PLUMED plugin. Bader charge analysis was used to obtain an approximation of the relative charges associated with individual atoms.[35,36]

3. RESULTS AND DISCUSSION

On the basis of our recent works, both experimental and computational, hydroxylated indium dioxide has been demonstrated to reduce CO_2 via the reverse water-gas shift (RWGS) reaction.[19] In these works, the presence of O vacancies, surface hydroxyl groups, and coordinately unsaturated surface indium atoms was found to be the necessary chemical environment necessary to drive the RWGS reaction. Our ground-state DFT analysis revealed the active sites and activation energy barriers for different steps of this reaction over defected indium sesquioxide.

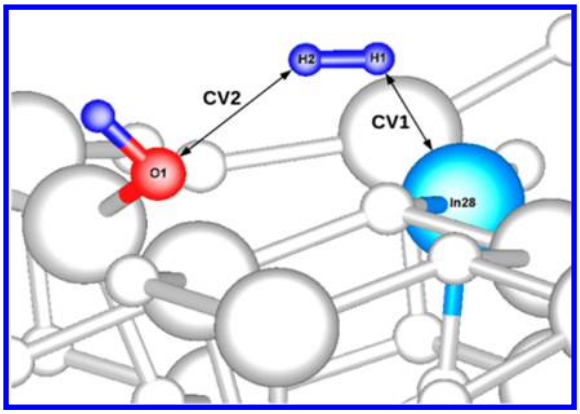

Figure 2. CVs used to define the free energy surface. CV1 is defined as the distance from the Lewis acid acting In (In28) to the nearest H (H1) on the adsorbate hydrogen molecule, while CV2 corresponds to the distance from O on the surface hydroxyl group (O1) to the other H (H2).

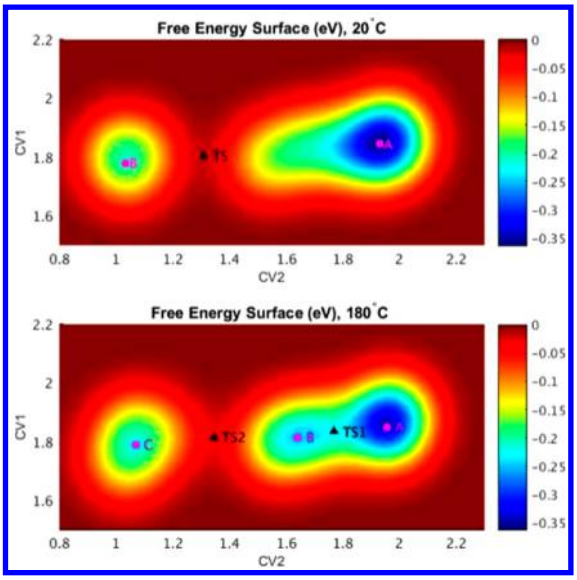

Figure 3. Free energy surfaces generated from MetaD-biased AIMD simulations for H_2 dissociation at 20 °C (top) and 180 °C (bottom). Points A and B denote locations of energy minima, and triangles TS denote locations of transition states.

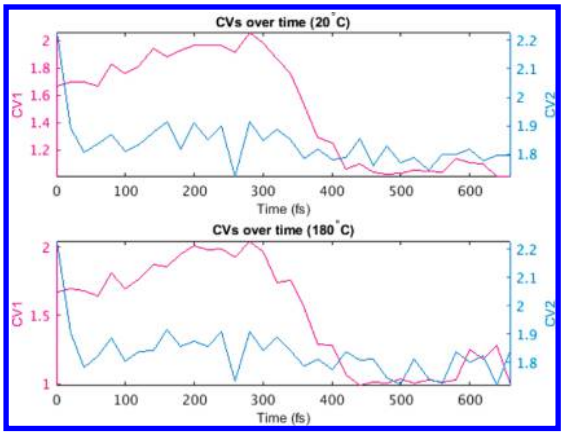

Figure 4. Evolution of CV1 and CV2 from MetaD-biased AIMD simulations for H_2 dissociation at 20 °C (top) and 180 °C (bottom).

The RWGS reaction mechanism over $In_2O_{3-x}(OH)_y$ has previously been identified to occur via two steps: H_2 is first dissociately adsorbed by the surface FLP site, and CO_2 is subsequently adsorbed and dissociated. In order to capture the details of each reaction step, separate MetaD-biased simulations were performed for H_2 splitting and CO_2 reduction.

3.1. Hydrogen Splitting via Surface FLP. The dissociation of H_2 over the catalyst surface at 20 and 180 °C was investigated using well-tempered MetaD-biased AIMD. Several test runs were first performed to optimize the various simulation parameters: i.e. the number and type of collective variables, the molecular dynamics time step, and the height and width of the Gaussian bias potentials (see the Supporting Information). Two collective variables, CV1 and CV2, were selected to ensure a complete and relevant representation of the free energy surface. CV1 is defined as the distance from the Lewis acid acting In (labeled In28) on the surface to the nearest H (labeled H1) on the adsorbate hydrogen molecule, while

DOI: 10.1021/acscatal.6b01545
ACS Catal. 2016, 6, 7109−7117

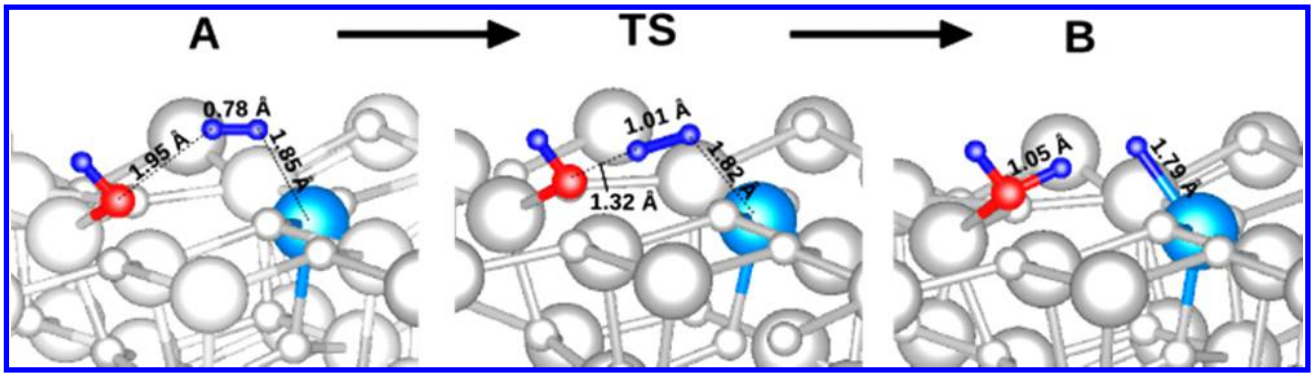

Figure 5. Atomic configurations corresponding to states A, TS, and C (Figure 3, top) for the dissociation of H_2 at 20 °C. Frame A corresponds to the reactant state, frame TS to the transition state, and frame C to the dissociated product state. Light blue denotes In, red denotes O, and dark blue denotes H.

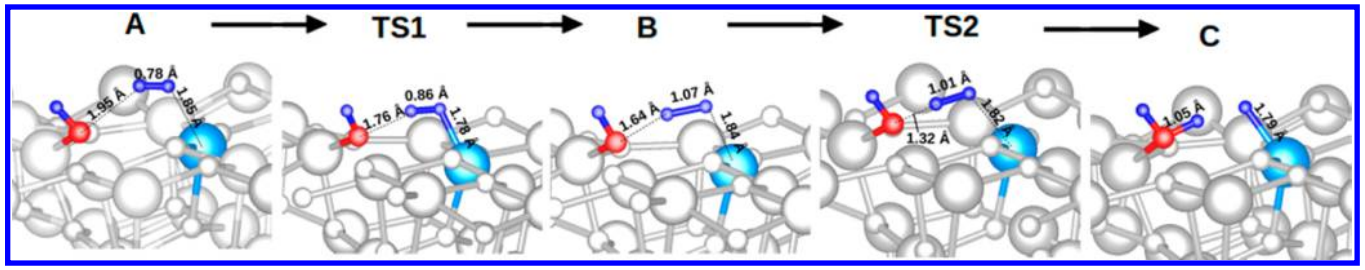

Figure 6. Atomic configurations corresponding to states A, TS1, B, TS2, and C (Figure 3, bottom) for the dissociation of H_2 at 180 °C. Frame A corresponds to the reactant state, frame B to the intermediate state, and frame C to the dissociated product state. Light blue denotes In, red denotes O, and dark blue denotes H.

Table 1. Bader Charge Analysis Comparing the Charge Associated with the Adsorbate Hydrogen Molecule (H1, H2) and the Lewis Acid (In) and Lewis Base (O) Sites on the Surface, Immediately before and after H_2 Dissociation, at 20 and 180 °C

	$In_2O_{3-x}(OH)_y$ and H_2 before splitting		$In_2O_{3-x}(OH)_y$ and H_2 after splitting	
	20 °C	180 °C	20 °C	180 °C
H1	−0.24	−0.22	−0.36	−0.37
H2	0.25	0.21	0.78	0.64
In	1.70	1.69	1.63	1.64
O	−1.24	−1.68	−1.87	−1.72

CV2 corresponds to the distance from O on the surface hydroxyl group (labeled O1) to the other H (labeled H2) on the adsorbate hydrogen molecule, as shown in Figure 2.

The free energy surface (Figure 3, top) corresponding to 20 °C shows the dissociative adsorption of hydrogen to have an energetic barrier of 0.36 eV and a Gibbs free energy of reaction of 0.16 eV. This matches with previously reported results that were derived from ground-state DFT reaction path finding methods that showed the dissociative adsorption of H_2 on $In_2O_{3-x}(OH)_y$ to be endothermic. The evolution of CV1 and CV2 during the reaction is presented in the top panel of Figure 4; plots of the simulation temperature over time are shown in Figure S2 in the Supporting Information. In this mechanism, the hydrogen molecule approaches the surface FLP site until it becomes sufficiently polarized and dissociates, at which point the hydrogen moieties become bound to oxygen on a surface hydroxyl group and to a neighboring surface indium atom, as shown in Figure 5. The hydrogen molecule floating over the catalyst surface has an initial bond length of 0.78 Å (frame A in Figure 5) and becomes stretched to 1.01 Å at the transition state (TS in Figure 5), at which point it dissociates into two H atoms, which susequently get attached to the OH group and the neighboring In sites, respectively, as shown in frame B. In agreement with previously reported ground-state DFT results,[19] Bader charge analysis, which is further discussed below, revealed the dissociation of H_2 to be heterolytic in nature.

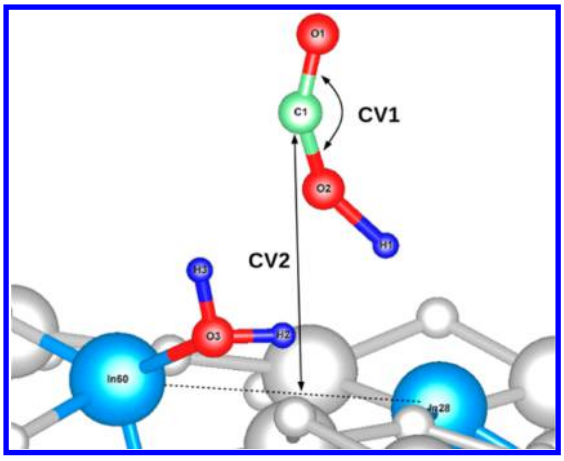

Figure 7. CVs used to define the free energy surface of the adsorption and reduction of CO_2 over $In_2O_{3-x}(OH)_y$ reaction. CV1 is defined as the angle formed by O1, C1, and O2, and CV2 is the distance from C1 to the midpoint between In28 and In60.

At a higher temperature of 180 °C, the dissociation of the H_2 molecule was found to proceed in two substeps, as shown in Figure 6. Plots showing the evolution of CV1 and CV2 during the reaction are presented in the bottom panel of Figure 4.

DOI: 10.1021/acscatal.6b01545
ACS Catal. 2016, 6, 7109−7117

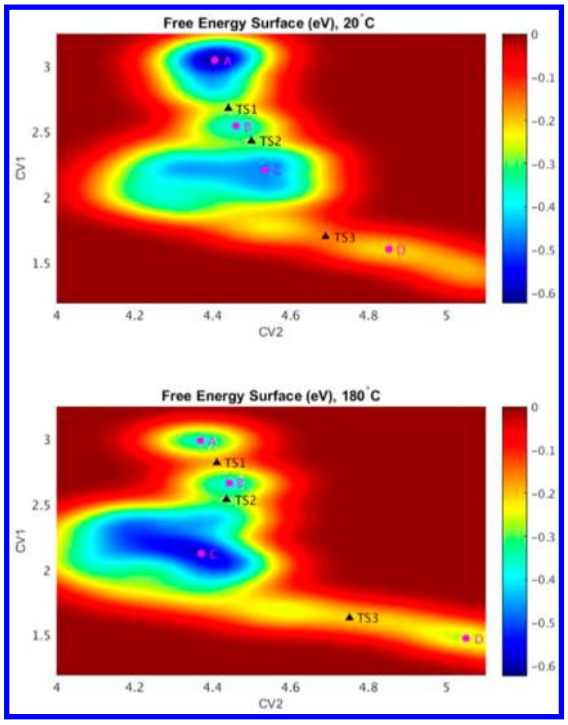

Figure 8. Free energy surfaces generated using MetaD-biased AIMD simulations for the adsorption and reduction of CO_2 over $In_2O_{3-x}(OH)_y$ at 20 °C (top) and 180 °C (bottom). Points A–D denote locations of energy minima, and triangles TS1–TS3 denote locations of the transition states.

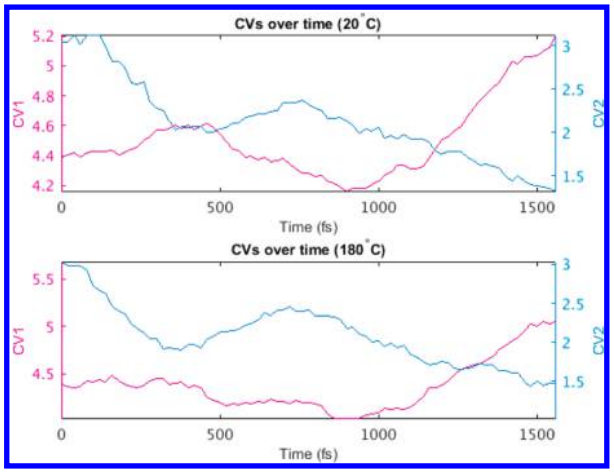

Figure 9. Evolution of CV1 and CV2 from MetaD-biased AIMD simulations for the adsorption and reduction of CO_2 over $In_2O_{3-x}(OH)_y$ at 20 °C (top) and 180 °C (bottom).

The H_2 adsorbate first approaches the surface and interacts with the Lewis-acting surface In atom to form a transition state in which the H_2 bond is stretched to 0.86 Å (TS1 in Figure 6). The distance from H_2 to the surface In is subsequently reduced (1.84 Å), while the distance to the surface hydroxyl group is further dimished (1.64 Å), forming a stable intermediate that was not observed at 20 °C (B in Figure 6). An explanation for the presence of an intermediate state at 180 °C is offered below. From intermediate state B, the reaction proceeds over a second transition state (TS2 in Figure 6), similarly to the mechanism at 20 °C. The H_2 molecule subsequently dissociates, and the resulting fragments are bound to the surface Lewis acid and Lewis base sites, identical with the room-temperature mechanism, reported before.[19] The free energy surface (Figure 3, bottom) shows that these substeps have energy barriers of 0.11 and 0.20 eV, respectively. The Gibbs free energy of reaction in the net reaction is 0.13 eV, suggesting that the reaction proceeds more favorably at 180 °C, which agrees with previously reported experimentally derived temperature-dependent rate measurements.[19]

According to transition state theory, the increased likelihood of the adsorbate colliding with the surface due to temperature is not expected to influence the topology of the free energy surface. Indeed, the appearance of an intermediate reaction step reveals a difference in the nature of the interaction between the adsorbate hydrogen molecule and the surface FLP site at higher temperature. To understand this further, two unbiased AIMD simulations were performed, one at 20 °C and the other at 180 °C, over 584 ps to compare the evolution of the FLP structure. The distance from the Lewis base acting O on the hydroxyl group to the Lewis acting indium atom was tracked over the course of the simulations to obtain a time-average FLP bond length. As expected by Boltzmann statistics, the fluctuations in FLP bond length were slightly greater in the higher temperature simulation (0.04 Å at 20 °C, in comparison to 0.05 Å at 180 °C); however, the time-average FLP bond length was also found to increase, from 3.35 Å at 20 °C to 3.39 Å at 180 °C, indicating a thermally induced change to the lattice structure. The alteration to the free energy surface for the dissociation of H_2 at 180 °C can likely be attributed to the enhanced separation of the surface FLP resulting at this temperature. To confirm this, the FLP bond distance was measured to be 3.28 Å at the intermediate state that appears at 180 °C (state B, Figure 6), whereas the structure corresponding to the equivalent set of CVs at 20 °C has an FLP bond distance of 3.25 Å. While this difference in bond length might appear minute, it is, to the best of our knowledge, the largest observable difference between equivalent regions of the free energy space at 20 and 180 °C and may therefore be the key to creating the conditions for the intermediate state that appears at 180 °C (B in Figure 6).

At both temperatures, the region of the free energy surface relevant to the dissociation of H_2 was observed to be dependent on CV2 (i.e., the distance from the O on the surface –OH group to nearest H on H_2) and independent of CV1 (i.e., the distance from the surface In to the nearest H on H_2). The terminally bonded nature of the surface hydroxyl group enables it with greater rotational degrees of freedom in comparison to the highly coordinated Lewis acid acting In that is embedded in the top layer of the lattice structure. The movement of the surface hydroxyl group is therefore more likely to drive the increase in separation between the FLP that results at higher temperature, in comparison to the surface In site. This view offers an explanation for the distance between the hydrogen molecule and the surface hydroxyl group (CV2) being the reaction-driving variable.

Bader charge analysis conducted immediately prior to hydrogen dissociation reveals that the Lewis acidic In and Lewis basic O of the OH sites at the surface possess charges of +1.70e and −1.24e at 20 °C and +1.69e and −1.68e at 180 °C (see Table 1). The frustrated charges of the surface FLP pair generate an electric field that polarizes the H molecule as it approaches the surface. The nearby H, being more positively charged than the Lewis acid acting In, accepts the excess charge from the latter and thus attains negative charges of −0.36e and

DOI: 10.1021/acscatal.6b01545
ACS Catal. 2016, 6, 7109–7117

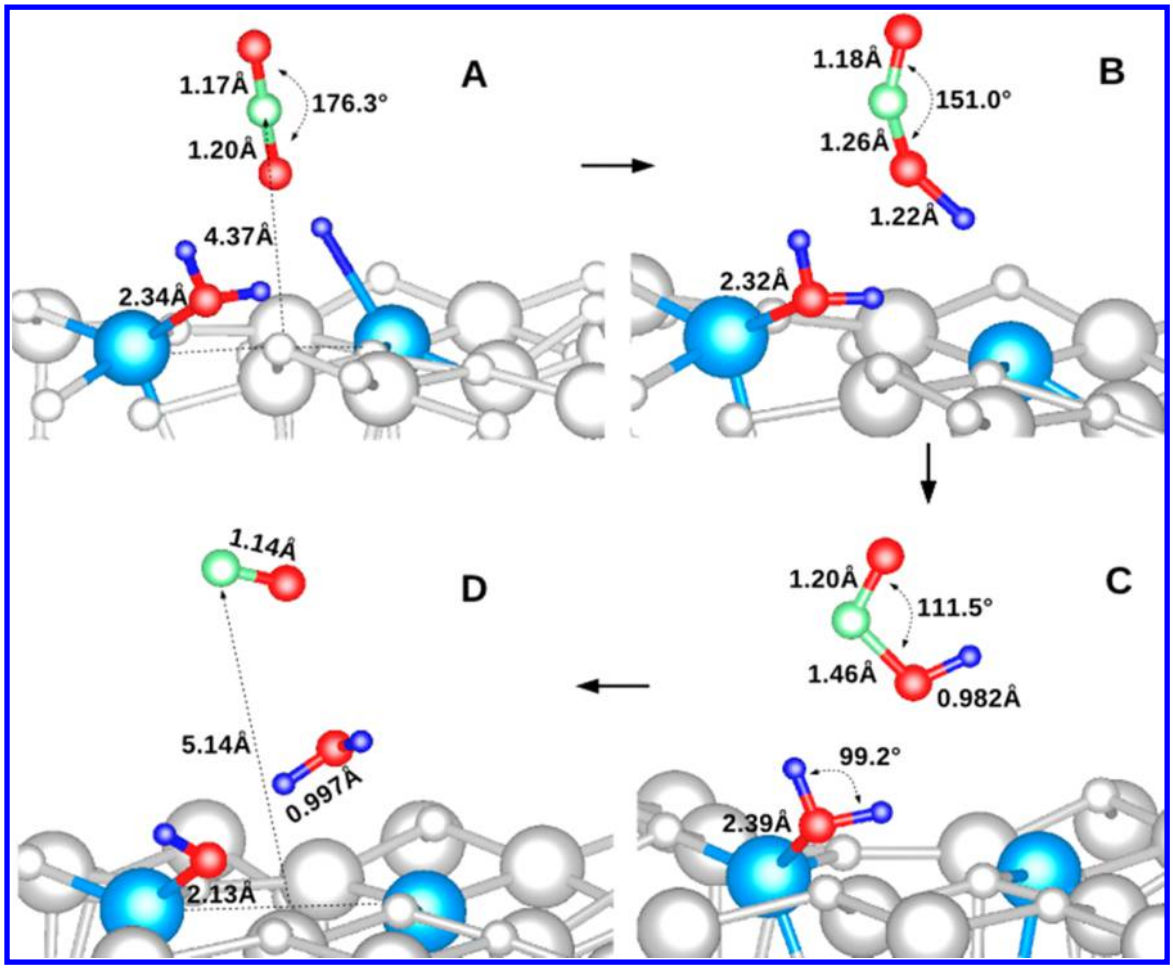

Figure 10. Atomic configurations corresponding to states A–D (Figure 8) for the adsorption and reduction of CO_2 at 20 °C. Light blue denotes In, red denotes O, and dark blue denotes H.

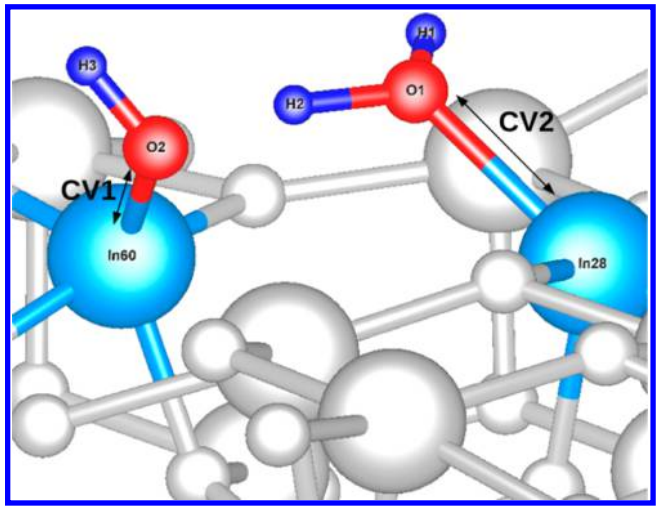

Figure 11. CVs used to define the free energy surface. CV1 is defined as the distance from In60 on the surface to O2, while CV2 is the distance from In28 to O1.

−0.37e at 20 and 180 °C, respectively. The other H, being closer to the Lewis base acting O on the surface −OH group, is more negatively charged and donates its charge to obtain charges of +0.78e and +0.64e at 20 and 180 °C, respectively. These results confirm the heterolytic nature of H_2 splitting and match those previously reported[19] for the ground-state mechanism.

The charge present on the Lewis acid acting In remains very consistent with temperature. While the O on the Lewis base acting hydroxide appears more negatively charged (−1.68e) at 180 °C, the net charge of the hydroxyl group (i.e. the combined charge of O and H on OH) does not change with temperature (−0.64e and −0.69e at 20 and 180 °C, respectively).

3.2. CO_2 Adsorption and Dissociation at the $In_2O_{3-x}(OH)_y$ surface. The subsequent step in the RWGS catalytic reaction proposed by Ghuman et al.[19] is the capture and reduction of CO_2 at the $In_2O_{3-x}(OH)_y$ surface. This reaction was also investigated at 20 and 180 °C using well-tempered MetaD-biased AIMD. Test simulations were first performed to optimize the various simulation parameters, as the dissociation of H_2 (see the Supporting Information). The two CVs that capture the energetics of this reaction are shown in Figure 7: CV1 corresponds to the angle formed by the CO_2 molecule (specifically, the angle formed by O1, C1, and O2), while CV2 is the distance from C1 to the midpoint between two neighboring surface indium atoms (labeled In28 and In60). A series of simulations were performed to capture the free energy surface of the adsorption and reduction of CO_2. Similar to the case for H_2 dissociation, simulations were first performed with the purpose of roughly exploring the free energy surface, followed by others to achieve finer treatment of the region of interest. The free energy surfaces generated (Figure 8) reveal

DOI: 10.1021/acscatal.6b01545
ACS Catal. 2016, 6, 7109–7117

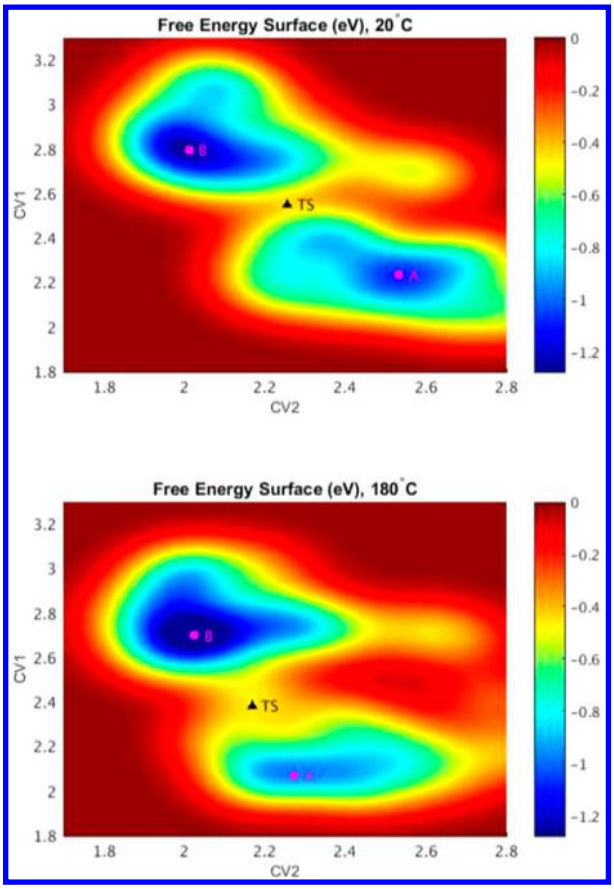

Figure 12. Free energy surfaces generated from MetaD-biased AIMD simulations for H_2O adsorption on the surface of $In_2O_{3-x}(OH)_y$ at 20 °C (top) and 180 °C (bottom). Points A and B indicate locations of energy minima, and triangles TS indicate the locations of a transition state.

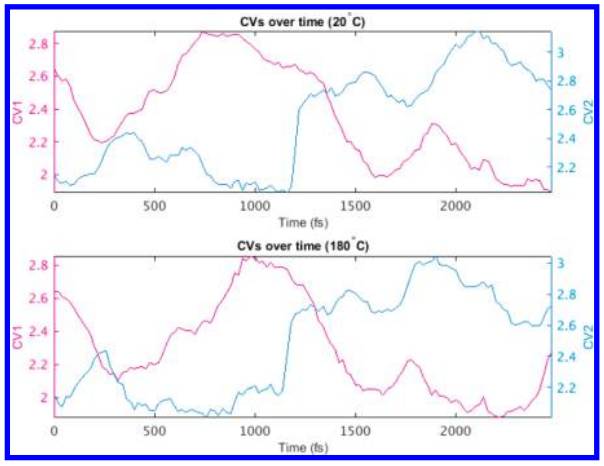

Figure 13. Evolution of CV1 and CV2 from MetaD-biased AIMD simulations for H_2O adsorption on the surface $In_2O_{3-x}(OH)_y$ at 20 °C (top) and 180 °C (bottom).

no significant change in the reaction mechanism between 20 and 180 °C, other than minor differences in the energetic barrier heights. At both 20 and 180 °C, the entire reaction is achieved in three steps that correspond to CO_2 adsorption, deformation, and ultimate dissociation, with transition states indicated by TS1, TS2, and TS3 in Figure 8. Plots showing the evolution of CV1 and CV2 during the reaction are presented in Figure 9; plots showing the simulation temperature over time are shown in Figure S7 in the Supporting Information. Under both temperature conditions, the linear CO_2 adsorbate molecule approaches the surface and inserts into the In−H bond (Figure 10), which was produced by the previous dissociative adsorption of hydrogen. It is interesting to note that, by this description, the reaction follows an Eley−Rideal mechanism, as the adsorbate−surface interactions are required to proceed in sequence.

The excess electrons on the hydride interact with the nucleophilic O on CO_2, causing the C−O bond to lengthen from 1.20 Å (state A) to 1.26 Å (state B) and finally to 1.46 Å (state C). The destabilization of CO_2 is further characterized by the bending of the O−C−O bond, from 176° (state A) to 151° (state B) and finally to 112° (state C), at which point the molecule splits to produce H_2O and CO. These findings are consistent with the ground-state DFT results[19] that showed the initially linear CO_2 bond angle to become 125.2° and the C−O bond to lengthen to 1.29 Å.

The topology of the free energy surface at 180 °C shows a slightly widened reaction pathway in comparison to that at 20 °C (Figure 8), displaying the expected increase in thermal vibrations, as k_BT is equal to 0.025 eV at 20 °C and 0.039 eV at 180 °C. The energy barrier to transition from state A to state B (Figure 8) is higher at 20 °C (0.32 eV) in comparison to that at 180 °C (0.19 eV), which can be attributed to an increased likelihood of the adsorbate successfully colliding with the surface at higher temperature. The subsequent energy barriers, corresponding to TS2 and TS3 (Figure 8), do not differ sufficiently between 20 and 180 °C to observe a significant thermal effect, as the resolution of the free energy surfaces is limited by the height of the deposited Gaussian potentials. The energy barrier associated with the adsorption of CO_2 and its initial interaction with surface hydride is therefore found to be reduced at higher temperature, while the later barriers associated with the bending and splitting of the CO_2 molecule remain mostly unchanged, suggesting that thermal effects may be relevant only when adsorptive mechanisms are involved. In agreement with previously reported results,[19] CO_2 adsorption and dissociation is found to be the rate-limiting step of the reaction, with the sum of the three energetic barriers being 0.93 and 0.63 eV at 20 and 180 °C, respectively. The Gibbs free energy of the net reaction is remarkably reduced from 0.41 eV at 20 °C to 0.10 eV at 180 °C, which matches previously reported experimental results showing the reaction to proceed more readily at higher temperatures.[19]

3.3. Dissociative Adsorption of H_2O. The desorption of H_2O is critical to guarantee sustained catalytic activity; water molecules bound to the surface, following CO_2 dissociation, will otherwise block catalytic sites and prevent subsequent reactions from taking place. Ghuman et al. report reduced CO production when H_2O was introduced into the reactor, under both batch and flow conditions, suggesting that product H_2O acts as a reaction inhibitor.[19] The interaction of H_2O with the $In_2O_{3-x}(OH)_y$ surface at both 20 and 180 °C was investigated using well-tempered MetaD-biased AIMD. Test runs were first performed to optimize the various aforementioned simulation parameters (see the Supporting Information), and two CVs over which to define the free energy surface were selected (Figure 11): CV1 is defined as the distance from In60 on the surface to O2, while CV2 is the distance from In28 to O1.

The reconstructed free energy surfaces are shown in Figure 12, and plots of CV1 and CV2 during the reaction are shown in

DOI: 10.1021/acscatal.6b01545
ACS Catal. 2016, 6, 7109−7117

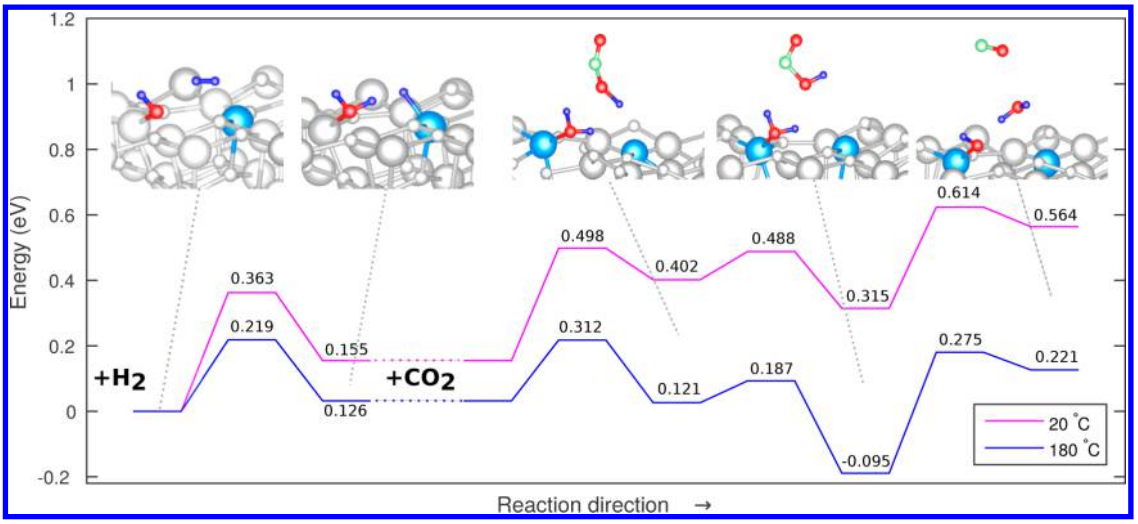

Figure 14. Summary of energetic barriers for the RWGS shift reaction over $In_2O_{3-x}(OH)_y$ at 20 °C (pink line) and 180 °C (blue line).

Figure 13. The time evolution of the simulation temperature is shown in Figure S9 in the Supporting Information.

The minimum reaction pathway traced from state A to B via TS corresponds to the transfer of H (on In-bound H_2O) to the neighboring surface hydroxyl group, effectively switching the positions of the surface-bound H_2O and OH groups by a proton-hopping process. The energy barriers corresponding to this step are found to be 0.68 eV at 20 °C and 0.52 eV at 180 °C, revealing the dissociative adsorption to be more favorable than direct desorption of H_2O from the surface. Such a result is consistent with previous first-principles studies that showed the dissociative chemisorption of H_2O to be favorable on the In_2O_3 surface.[37] From energy minimum A, energy barriers of at least 1.1 and 0.98 eV at 20 and 180 °C, respectively, must be overcome for desorption of H_2O to be achieved. Given that these barriers are greater than those the limiting the RWGS reaction, even when temperature conditions are considered, the blocking of catalytic sites by product H_2O is the likely mechanism preventing sustained catalytic activity over time. For practical purposes, this issue can be circumvented by careful design of a flow reactor in which the product water molecules are removed from the active catalyst surface.

4. CONCLUSION

In the present study, the effect of temperature on the surface FLP-driven RWGS reaction, leading to the experimentally observed formation of CO and H_2O, was investigated for the first time. Well-tempered MetaD-biased AIMD simulations were performed to probe the mechanism for the RGWS reaction over the $In_2O_{3-x}(OH)_y$ surface at temperatures of 20 and 180 °C. Free energy surfaces mapping the reaction pathways, transition states, and locations of energy minima were generated to obtain the energetics for the activation of hydrogen and the capture and reduction of carbon dioxide. The energy barrier associated with the activation of gaseous hydrogen over the surface FLP site was found to be reduced by 0.15 eV at 180 °C (blue line in Figure 14), which is substantially lower than at the ground state (pink line in Figure 14) reported before. Further AIMD results suggest that the surface FLP site is structurally altered under high-temperature conditions. In particular, the time-averaged distance between the Lewis acid acting In and the Lewis base acting O on the hydroxyl group was found to increase by 0.04 Å at 180 °C, which may provide conditions required to break the reaction into two smaller energetic steps (Figure 3). The reduction of gaseous CO_2 is found to be the rate-limiting step (Figure 14), with no significant change resulting from increased temperature conditions; however, the energy barrier corresponding to the adsorption of CO_2 is slightly reduced at 180 °C in comparison to that at 20 °C, suggesting that thermal effects may only be relevant to the reaction step characterized by adsorptive mechanisms. The dynamics of the product H_2O molecule over $In_2O_{3-x}(OH)_y$ was also investigated using well-tempered MetaD-biased AIMD. The free energy surface revealed dissociative adsorption of H_2O at the In and hydroxyl sites to be preferred over direct desorption from the surface, at both 20 and 180 °C. The desorption of H_2O was found to have energetic barriers of 1.1 and 0.98 eV, at 20 and 180 °C, respectively, which strongly suggests that product H_2O prevents sustained catalytic activity by blocking surface sites. The overall reaction is found to be endergonic, which is in agreement with previous experimental and theoretical studies.[19] These results attest to the interesting catalytic mechanisms enabled by of surface FLP chemistry: in particular, the heterogeneous reduction of CO_2.

■ ASSOCIATED CONTENT

Supporting Information

The Supporting Information is available free of charge on the ACS Publications website at DOI: 10.1021/acscatal.6b01545.

Background into metadynamics, PLUMED plugin parameters, plots of simulation temperature over time, and initial atomic coordinates for all MetaD-biased AIMD simulations (PDF)

■ AUTHOR INFORMATION

Corresponding Author

*E-mail for C.V.S.: chandraveer.singh@utoronto.ca.

Notes

The authors declare no competing financial interest.

■ ACKNOWLEDGMENTS

Financial support for this work was provided by the Natural Sciences and Engineering Research Council of Canada (NSERC), Ontario Ministry of Research Innovation (MRI),

DOI: 10.1021/acscatal.6b01545
ACS Catal. 2016, 6, 7109−7117

Ministry of Economic Development, Employment and Infrastructure (MEDI), Ministry of the Environment and Climate Change, Connaught Innovation Fund, and the Connaught Global Challenge Fund. Computations were carried out at Compute Canada facilities Calcul-Quebec and SciNet; C.V.S. gratefully acknowledges their continued support. G.A.O. is Government of Canada Research Chair in Materials Chemistry and Nanochemistry.

REFERENCES

(1) Olah, G. A.; Goeppert, A.; Surya Prakash, G. K. *J. Org. Chem.* **2009**, *74*, 487−498.
(2) Aresta, M. Wiley-VCH: Weinheim, Germany, 2010.
(3) Ozin, G. *Adv. Mater.* **2015**, *27*, 1957−1963.
(4) Centi, G.; Quadrelli, E. A.; Perathoner, S. *Energy Environ. Sci.* **2013**, *6*, 1711−1731.
(5) Qiao, J.; Liu, Y.; Hong, F.; Zhang, J. *Chem. Soc. Rev.* **2014**, *43*, 631−675.
(6) Stephan, D. W.; Erker, G. *Angew. Chem., Int. Ed.* **2015**, *54*, 6400−6441.
(7) Rokob, T. A.; Hamza, A.; Stirling, A.; Soós, T.; Pápai, I. *Angew. Chem., Int. Ed.* **2008**, *47*, 2435−2438.
(8) Stephan, D. W.; Erker, G. *Angew. Chem., Int. Ed.* **2010**, *49*, 46−76.
(9) Stephan, D. W. Frustrated Lewis Pairs. *J. Am. Chem. Soc.* **2015**, *137*, 10018−10032.
(10) Mömming, C. M.; Otten, E.; Kehr, G.; Fröhlich, R.; Grimme, S.; Stephan, D. W.; Erker, G. *Angew. Chem., Int. Ed.* **2009**, *48*, 6643−6646.
(11) Zhao, X.; Stephan, D. W. *Chem. Commun.* **2011**, *47*, 1833−1835.
(12) Courtemanche, M.-A.; Légaré, M.-A.; Maron, L.; Fontaine, F.-G. *J. Am. Chem. Soc.* **2014**, *136*, 10708−10717.
(13) Ménard, G.; Stephan, D. W. *J. Am. Chem. Soc.* **2010**, *132*, 1796−1797.
(14) Sgro, M. J.; Domer, J.; Stephan, D. W. *Chem. Commun.* **2012**, *48*, 7253−7255.
(15) Ashley, A. E.; Thompson, A. L.; O'Hare, D. *Angew. Chem., Int. Ed.* **2009**, *48*, 9839−9843.
(16) Berkefeld, A.; Piers, W. E.; Parvez, M. *J. Am. Chem. Soc.* **2010**, *132*, 10660−10661.
(17) Ménard, G.; Stephan, D. W. *Angew. Chem.* **2011**, *123*, 8546−8549.
(18) Hoch, L. B.; Wood, T. E.; O'Brien, P. G.; Liao, K.; Reyes, L. M.; Mims, C. A.; Ozin, G. A. *Adv. Sci.* **2014**, *1*, 1400013.
(19) Ghuman, K. K.; Wood, T. E.; Hoch, L. B.; Mims, C. A.; Ozin, G. A.; Singh, C. V. *Phys. Chem. Chem. Phys.* **2015**, *17*, 14623−14635.
(20) Ghuman, K. K.; Hoch, L. B.; Szymanski, P.; Loh, J.; Kherani, N.; El-Sayed, M.; Ozin, G. A.; Singh, C. V. *J. Am. Chem. Soc.* **2016**, *138*, 1206−1214.
(21) Poznyak, S. K.; Golubev, A. N.; Kulak, A. I. *Surf. Sci.* **2000**, *454*−*456*, 396−401.
(22) Bielz, T.; Lorenz, H.; Jochum, W.; Kaindl, R.; Klauser, F.; Klotzer, B.; Penner, S. *J. Phys. Chem. C* **2010**, *114*, 9022−9029.
(23) Du, N.; Zhang, H.; Chen, B. D.; Ma, X. Y.; Liu, Z. H.; Wu, J. B.; Yang, D. R. *Adv. Mater.* **2007**, *19*, 1641−1645.
(24) Lorenz, H.; Jochum, W.; Klötzer, B.; Stöger-Pollach, M.; Schwarz, S.; Pfaller, K.; Penner, S. *Appl. Catal., A* **2008**, *347*, 34−42.
(25) Barducci, A.; Bussi, G.; Parrinello, M. *Phys. Rev. Lett.* **2008**, *100*, 020603.
(26) Barducci, A.; Bonomi, M.; Parrinello, M. *WIREs Comput. Mol. Sci.* **2011**, *1*, 826−843.
(27) Ghuman, K. K.; Yadav, S.; Singh, C. V. *J. Phys. Chem. C* **2015**, *119*, 6518−6529.
(28) Urakawa, A.; Iannuzzi, M.; Hutter, J.; Baiker, A. *Chem. - Eur. J.* **2007**, *13*, 6828−6840.
(29) Kumar, P. P.; Kalinichev, A. G.; Kirkpatrick, R. J. *J. Chem. Phys.* **2007**, *126*, 204315.
(30) Brüssel, M.; di Dio, P. J.; Muñiz, K.; Kirchner, B. *Int. J. Mol. Sci.* **2011**, *12*, 1389−1409.
(31) Giannozzi, P.; Baroni, S.; Bonini, N.; Calandra, M.; Car, R.; Cavazzoni, C.; Ceresoli, D.; Chiarotti, G. L.; Cococcioni, m.; Dabo, I.; Dal Corso, A.; Fabris, S.; Fratesi, G.; de Gironcoli, S.; Gebauer, R.; Gerstmann, U.; Gougoussis, C.; Kokalj, A.; Lazzeri, M.; Martin-Samos, L.; Marzari, N.; Mauri, F.; Mazzarello, R.; Paolini, S.; Pasquarello, A.; Paulatto, L.; Sbraccia, C.; Scandolo, S.; Sclauzero, G.; Seitsonen, A. P.; Smogunov, A.; Umari, P.; Wentzcovitch, R. M. *J. Phys.: Condens. Matter* **2009**, *21*, 395502.
(32) Perdew, J. P.; Burke, K.; Ernzerhof, M. *Phys. Rev. Lett.* **1996**, *77*, 3865−3868.
(33) Kresse, G.; Joubert, D. *Phys. Rev. B: Condens. Matter Mater. Phys.* **1999**, *59*, 1758.
(34) Zhang, K. H. L.; Walsh, A.; Catlow, C. R. A.; Lazarov, V. K.; Egdell, R. G. *Nano Lett.* **2010**, *10*, 3740−3746.
(35) Henkelman, G.; Arnaldsson, A.; Jónsson, H. *Comput. Mater. Sci.* **2006**, *36*, 354−360.
(36) Sanville, E.; Kenny, S. D.; Smith, R.; Henkelman, G. *J. Comput. Chem.* **2007**, *28*, 899−908.
(37) Zhou, C.; Li, J.; Chen, S.; Wu, J.; Heier, K. R.; Cheng, H. *J. Phys. Chem. C* **2008**, *112*, 14015−14020.

DOI: 10.1021/acscatal.6b01545
ACS Catal. 2016, 6, 7109−7117